SLAC–PUB–5840
May 1992
(T/E)

MEASUREMENTS OF νW_2 AND $R = \sigma_L/\sigma_T$ FROM INELASTIC ELECTRON-ALUMINUM SCATTERING NEAR $x = 1$*

P. E. Bosted,[1] A. Lung,[1] L. Andivahis,[1] L. M. Stuart,[2,4] J. Alster,[12]
R. G. Arnold,[1] C. C. Chang,[5] F. S. Dietrich,[4] W. Dodge,[7] R. Gearhart,[10]
J. Gomez,[3] K. A. Griffioen,[8] R. S. Hicks,[6] C. E. Hyde-Wright,[13] C. Keppel,[1]
S. E. Kuhn,[11] J. Lichtenstadt,[12] R. A. Miskimen,[6] G. A. Peterson,[6]
G. G. Petratos,[9,a] S. E. Rock,[1] S. Rokni,[6,a] W. K. Sakumoto,[9]
M. Spengos,[1] K. Swartz,[13] Z. Szalata,[1] L. H. Tao[1]

[1] *The American University, Washington, D.C. 20016*
[2] *University of California, Davis, California 95616*
[3] *CEBAF, Newport News, Virginia 23606*
[4] *Lawrence Livermore National Laboratory, Livermore, California 94550*
[5] *University of Maryland, College Park, Maryland 20742*
[6] *University of Massachusetts, Amherst, Massachusetts 01003*
[7] *National Institute of Standards and Technology, Gaithersburg, Maryland 20899*
[8] *University of Pennsylvania, Philadelphia, Pennsylvania 19104*
[9] *University of Rochester, Rochester, New York 14627*
[10] *Stanford Linear Accelerator Center, Stanford, California 94309*
[11] *Stanford University, Stanford, California 94305*
[12] *University of Tel-Aviv, Ramat Aviv, Tel-Aviv 69978, Israel*
[13] *University of Washington, Seattle, Washington 98195*

Submitted to Physical Review C

---

*Work supported in part by National Science Foundation grants PHY–87–15050 (AU), PHY–89–18491 (Maryland), PHY–88–19259 (U Penn), and PHY–86–58127 (UW); by Department of Energy contracts DE–AC03–76SF00515 (SLAC), W–7405–ENG–48 (LLNL), DE–FG02–88ER40415 (U Mass), DE–AC02-ER13065 (UR) and DE–FG06–90ER40537 (UW); and by the US–Israel Binational Science Foundation.

ABSTRACT

Cross sections for inclusive electron scattering from aluminum have been measured at both forward and backward angles in the kinematic region near $x = 1$ and $1.75 < Q^2 < 7$ (GeV/c)^2. The forward angle data are in good agreement with a recent calculation. Both the data and the calculation show scaling behavior for $F_2(\xi, Q^2) = \nu W_2(\xi, Q^2)$ at high Q^2 for fixed values of the Nachtmann variable ξ. The ratio $R = \sigma_L/\sigma_T$ has been extracted for $1.75 < Q^2 < 5$ (GeV/c)^2 and is found to decrease with Q^2 to a value consistent with zero at the highest Q^2.

I. INTRODUCTION

Inelastic electron scattering from a nucleon or nucleus at large four-momentum transfer squared, Q^2, has been successfully used to study the longitudinal quark momentum distributions. The deep inelastic structure functions $F_2(x,Q^2) = \nu W_2(x,Q^2)$ and $F_1(x,Q^2) = MW_1(x,Q^2)$ become approximately independent of Q^2 at fixed x, in a phenomenon known as scaling, for $Q^2 > 2$ (GeV/c)^2 and $W^2 > 4$ (GeV)^2. The x variable is a measure of the longitudinal momentum carried by the struck partons, and is kinematically defined as $x = Q^2/2M\nu$, where M is the nucleon mass, and $\nu = E - E'$ is the energy transferred by an electron of initial energy E and final energy E'. The mass of the final state squared is defined by $W^2 = M^2 + 2M\nu - Q^2$. Logarithmic scaling violations are well-described by perturbative QCD (pQCD), while at low Q^2 corrections proportional to $1/Q^2$ are needed to account for target-mass and higher twist effects. For $W^2 < 4$ (GeV)^2, various nucleon resonances become important, but Bloom and Gilman [1] found that the resonance form factors averaged over a finite range in x fall at the same rate as the deep inelastic structure functions. This local duality was shown [2] to follow from pQCD, even for the nucleon elastic peak at $x = 1$. It was also demonstrated that the effect of the finite target mass can be removed by analyzing the structure functions in terms of the Nachtmann variable $\xi = 2x/[1 + (1 + 4M^2x^2/Q^2)^{1/2}]$, which approaches x at high Q^2.

Previous experiments [3,4] have studied inelastic scattering from heavy nuclei at moderate Q^2 (greater than 1 (GeV/c)^2) and large ξ ($\xi > 0.6$), and have observed approximate scaling [5] of the forward-angle structure function νW_2 when examined as a function of Q^2 at fixed ξ. These data extend well beyond the resonance region to include substantial contributions from quasielastic scattering near $x = 1$, for which the elastic channel is widened by the Fermi motion of the nucleons. Microscopic models [6,7] have been able to reproduce the detailed ξ- and

Q^2-dependence of the previous forward-angle data on iron by convoluting the inelastic and elastic structure functions for free nucleons with spectral functions that describe the momentum and energy distribution of the bound nucleons.

The present experiment provides additional data on aluminum in the range $1.75 < Q^2 < 7$ (GeV/c)^2, allowing detailed comparison with the microscopic models. The ratio of aluminum to deuterium cross sections will also be examined, since this experiment also measured electron scattering from deuterium. A new feature of the present experiment is that data were taken at both forward and backward angles, permitting for the first time the extraction of $R = \sigma_L/\sigma_T$, the ratio of longitudinal and transverse photoabsorption cross sections. These data are used to test the expectation [2] that R should be small and approach zero at high Q^2 if scattering takes place primarily from spin-1/2 objects in the nucleus.

II. THE EXPERIMENT

The experiment, known as NE11, consisted of measuring the differential cross sections for scattering electrons from an aluminum target at several scattering angles and beam energies. The aluminum measurements were not the primary focus of the experiment, which measured the elastic form factors of the proton [8] using *ep* elastic scattering and the elastic form factors for the neutron [9] using quasielastic electron scattering from the deuteron. The Nuclear Physics Injector at the Stanford Linear Accelerator provided electron beams with energies from 1.5 to 5.5 GeV in the non-SLED mode at average currents from 0.5 to 10 μA, and at 9.8 GeV in the SLED mode at an average current of 2 μA. The beam pulses were 2 μsec long in the non-SLED mode, and 0.15 μsec long in the SLED mode. The pulse repetition rate was 120 Hz. The beam steering system kept the beam centered on the target to within 1 mm, with an angle with respect to the nominal beam axis of less than 0.05 mr. The integrated charge was independently measured by two toroid monitors, which typically agreed with each other to within 0.2%.

The response of each monitor was determined every few hours with a precision capacitor calibration system. The absolute gain was known to better than $\pm 0.5\%$.

The target consisted of two 0.63 mm thick pieces of aluminum spaced 15 cm apart and oriented at an angle of 45° with respect to the beam axis, providing a total effective thickness of 1.8 mm, or 0.02 radiation lengths (r.l.). This target was primarily designed to measure contributions from the aluminum endcaps of the liquid hydrogen and deuterium targets, rather than for absolute aluminum cross section measurements. The error on the target thickness is estimated to be $\pm 2\%$.

Electrons scattered from aluminum were detected in the SLAC 8 GeV/c spectrometer [10] which was set at central electron scattering angles, θ, between 15° and 90°, and central momenta, E', between 0.5 and 7.5 GeV/c. The detector package was designed to determine particle trajectories and to distinguish electrons from a large flux of pions and other backgrounds. It included a 99.9% efficient gas Čerenkov counter (Č) filled with 0.6 atmospheres of nitrogen and a 99.7% efficient lead glass shower counter array with a resolution of $\pm 8\%/\sqrt{E'}$. The lead glass array was segmented longitudinally into a 3 r.l. preradiator (PR) and total absorber (TA) blocks totalling 13.2 r.l. (19.8 r.l. above $E' = 4$ GeV). These detectors together provided a pion rejection power of about 1:10,000 at low E', where the background was largest. Ten planes of multi-wire proportional chambers were used to measure particle track coordinates with an efficiency of 99.9%. The trajectories were used to determine the scattered electron momentum to $\pm 0.15\%$ and the electron scattering angle to ± 0.5 mr. Four planes of scintillators (SF, SM, HX, HY) were used for triggering and to help resolve track ambiguities.

The detector phototube pulse heights and arrival times were measured with standard CAMAC ADCs and TDCs. A CAMAC serial readout module was used for the wire chambers. The CAMAC modules were read out by a PDP-11 computer, which stored the results directly into the memory of a VAX 11/780 computer. Discriminators and coincidence circuits were used to form two types of

triggers: electron and pion triggers. Electron triggers consisted of either a coincidence of $\check{C}$ with at least two of PR, SF, or SM, or a coincidence of at least three of $\check{C}$, PR, TA, or SM. The pion trigger required a coincidence of SF and SM, both with thresholds low enough to be efficient for pions, and the absence of a $\check{C}$ signal. The pion trigger was pre-scaled, so that only a sample of pions were analyzed. The computer could only analyze the first trigger in a given beam pulse, but all triggers were counted by CAMAC scalers, so that a correction for computer dead-time could be made.

Monte Carlo simulations were used to determine the acceptance of the spectrometer as a function of relative momentum δ, relative horizontal scattering angle $d\theta$, and vertical angle ϕ. The Monte Carlo was based on a TRANSPORT [11] model derived from floating-wire [12] optical coefficient measurements. These measurements determined the acceptance in the fiducial, aperture-free region ($|\delta| < 2\%$, $|d\theta| < 5$ mr, and $|\phi| < 10$ mr) to $\pm$ 1%. The angular dependence of the acceptance outside the fiducial region, as predicted by the Monte Carlo model, was checked by verifying that elastic cross sections measured from hydrogen were independent of ϕ and followed the expected dipole fit dependence on $d\theta$. The δ-dependence was checked by comparing high-statistics cross sections for inelastic scattering from deuterium measured with the same beam energy and spectrometer angle, but central momentum settings that differed by a few percent. Small adjustments to the positions of some of the apertures in the Monte Carlo model were made within the measured tolerances to achieve the best results for these tests. The Monte Carlo program was also used to determine the dependence of the acceptance function on central angle setting due to the 15 cm target length, and on central momentum setting due to the effects of multiple scattering on particle trajectory reconstruction.

Spectra at each kinematic point were obtained as a function of x at fixed θ by dividing the measured counts by the acceptance and using a model (see below) to correct for the cross-section variation within the small $d\theta$-range of the spectrometer.

The kinematics were well-defined for each point, since the uncertainties in E, E', and θ were only 0.05%, 0.05%, and 0.005° respectively. These uncertainties were verified by checking that the ep elastic peaks were centered at $x = 1$. Corrections were made to take into account the difference in ionization energy loss for the aluminum and hydrogen targets. Corrections of up to 5% at backward angles were made for pions misidentified as electrons, as determined from a study of the energy spectra in the lead glass shower counter. Corrections ($< 1\%$) were also made for the contribution of electrons from pair-production in the target, as measured by reversing the polarity of the spectrometer.

The final experimental cross sections were obtained by applying a correction for radiative processes, using the peaking approximation formulas of Tsai [13], with corrections as given by Bardin [14] for μ, τ, and quark vacuum loops, higher order terms in the fine-structure constant α, and radiation from quarks. The peaking approximation is expected to be valid at the 1% to 2% level in our kinematic region, so the full formulas which integrate over all emitted photon angles were not used. As input to the radiative correction formulas, we used a cross section model based on the forward-angle νW_2 calculations of Liuti [15] at Q^2=1.75, 2.5, 3.25, 4, 5, 6, and 7 (GeV/c)^2. These calculations were made for discrete values of x from 0.5 to 2, with a spacing of 0.1. As can be seen in Figs. 1 and 2, these calculations are in good agreement with our forward-angle, radiatively corrected data. To obtain νW_2 at any desired value of x and Q^2, linear interpolations in Q^2 and logarithmic interpolations in x were performed. Values of the backward-angle structure function W_1 were obtained assuming $R = \sigma_L/\sigma_T = [0.32\ (\mathrm{GeV/c})^2]/Q^2$, as will be justified below. The radiative correction factor sensitivity to other reasonable models for R was found to be small compared to the experimental error bars.

III. CROSS SECTIONS AND νW_2

The final experimental cross sections per nucleon are listed in Table 1 as a function of the kinematic variables E', Q^2, x, ξ, and photon longitudinal polarization $\epsilon = [1 + 2(1 + \nu^2/Q^2)\tan^2(\theta/2)]^{-1}$. The errors are statistical only, and do not include an overall normalization error of approximately 3%, obtained by combining the errors due to the spectrometer solid angle (1%), target thickness (2%), radiative corrections (2%), and beam current normalization (0.5%). Total point-to-point errors of typically 1% from the combination of uncertainties in E and θ, and possible variations in detector efficiency, spectrometer solid angle as a function of momentum, and dead-time corrections are also not included. In all cases the statistical error is larger than the total systematic error on any given data point.

The cross sections can be written in terms of two structure functions, W_1 and W_2, that depend only on x and Q^2 (or, equivalently, on ξ and Q^2):

$$\frac{d\sigma}{d\Omega dE'} = \sigma_M[W_2 + 2W_1 \tan^2(\frac{\theta}{2})], \tag{3.1}$$

where the Mott cross section is given by $\sigma_M = \alpha^2 \cos^2(\theta/2)/4E^2 \sin^4(\theta/2)$. In order to study the scaling behavior of the structure functions and make comparisons to calculations, it is useful to extract $F_2 = \nu W_2$ from the data using a model for the relationship between W_1 and W_2. If we define R as the ratio of cross sections for longitudinal and transverse photon polarization, then $W_1 = (1+\nu^2/Q^2)W_2/(1+R)$. This relation is particularly useful when R is small, as it is known to be in the deep-inelastic region [16]. In the quasielastic region and for an isoscalar target, the non-relativistic PWIA [17] can be used to determine R in terms of the elastic nucleon form factors:

$$R = \frac{\sigma_L}{\sigma_T} = \frac{4M^2(G_{Ep}^2 + G_{En}^2)}{Q^2(G_{Mp}^2 + G_{Mn}^2)}. \tag{3.2}$$

The nucleon elastic form factor measurements of the present experiment [8,9] show that, to a good approximation, the form factors follow the scaling law

$G_{Ep}(Q^2) = G_{Mp}(Q^2)/\mu_p = G_{Mn}(Q^2)/\mu_n$ and $G_{En} = 0$, where the proton and neutron magnetic moments are given by $\mu_p = 2.793$ nm and $\mu_n = -1.91$ nm. Using this scaling law, we obtain

$$R = \frac{4M^2}{Q^2(\mu_p^2 + \mu_n^2)} = \frac{0.32\ (\mathrm{GeV/c})^2}{Q^2}. \tag{3.3}$$

This expression was used to extract $\nu W_2/A$ from the cross section data and obtain the results listed in Table 1, where $A = 27$ is the atomic number for aluminum.

The extracted values of $\nu W_2/A$ are plotted as a function of ξ for the spectra at the two highest beam energies, E=5.5 and 9.8 GeV, in Figs. 1 and 2. These spectra were chosen because they span the largest ξ ranges, have the smallest statistical errors, and are at forward angles where the contributions from W_1 are very small. The spectra look similar, indicating an approximate scaling in the ξ variable. This would not have been the case if the x variable had been used, since it does not take into account the target mass corrections. A closer examination of the scaling behavior is shown in Fig. 3, where the interpolated values of $\nu W_2/A$ are plotted versus Q^2 at four values of ξ. Also shown are aluminum data at forward angles from previous SLAC experiments E139 [18] and E133 [4], and iron data from SLAC experiment NE3 [3]. The present experiment is in very good agreement with the previous data, including that for iron, when scaled by the number of nucleons, A. This is not surprising since the binding energy and spectral functions for aluminum and iron are similar. The value of Q^2 where scaling begins ($\nu W_2/A$ becomes independent of Q^2) grows from about 2 $(\mathrm{GeV/c})^2$ at $\xi = 0.6$ to about 5 $(\mathrm{GeV/c})^2$ at $\xi = 0.9$. In addition, a definite enhancement in $\nu W_2/A$ can be seen at low Q^2 for the higher ξ bins, due to the influence of the quasielastic peak. Scaling seems to begin above this enhancement, where the quasielastic contributions have died out.

The data are well-reproduced by the microscopic calculation of Liuti [15], shown as the solid lines in Figs. 1, 2, and 3. The quasielastic contributions are

shown as the short dashed lines. This calculation uses as input the Bodek [19] parametrization of the deep-inelastic and resonance region structure functions and nucleon elastic form factors in good agreement with those found from the proton and neutron measurements of this experiment [8,9] for the quasielastic contribution ($G_{Mp}/\mu_p = G_{Mn}/\mu_n = G_{Ep}$ where G_{Mp} is the Gari-Krümpelmann fit [20] and $G_{En} = 0$). The aluminum cross sections were obtained in the relativistic Plane-Wave Impulse Approximation (PWIA) by convoluting the free nucleon form factors and inelastic structure functions with a spectral function for aluminum that included two-nucleon correlations [21], and taking into account the difference between free and bound structure functions using the off-shell prescription of de Forest [22]. Other off-shell prescriptions give somewhat different results in the kinematic region of our experiment [6]. The convolution is done in the light-front dynamics formalism. Integration was done over both missing momentum and energy, since the closure approximation (integration only over momentum using an energy-integrated spectral function) gives significantly different results. The two-nucleon correlations were treated in two different ways: one which assumes the $(A-2)$ spectator is at rest; and one in which the relative motion is taken into account. These two methods were found to give essentially the same results. The effects of final-state interactions (FSI) and meson-exchange currents (MEC) were not taken into account. While importance of FSI is likely to decrease with Q^2 at fixed ξ, the influence of MEC could remain substantial at high Q^2, and would be a good topic for further investigation.

It is of some interest to compare the cross section for aluminum to those for the lightest nucleus, deuterium. It was observed previously [4] that the much larger Fermi-momentum in aluminum causes the quasielastic peak to be considerably wider than in deuterium, and the inelastic tail has considerably more strength at very large ξ or x. These observations can readily explain the experimental cross section ratios, shown in Fig. 4 for the Q^2 values where data were taken on

deuterium at forward angles. The dip at $x = 1$, where the quasielastic peak is located, is gradually filled in at higher Q^2, where the quasielastic contributions become less important. The peak seen at $x < 1$ also disappears with increasing Q^2 as the dip region between the quasielastic peak and the $\Delta(1236)$ resonance becomes filled in. The ratio near $x = 0.8$ drops below 1 at the higher Q^2, in agreement with the well-known classic EMC effect [18]. At high x, the ratio of aluminum to deuterium is always greater than 1, and appears to increase with x for all values of Q^2. This trend is due to the larger Fermi momentum for aluminum. The exact magnitude is influenced by final-state interactions and possible two-nucleon correlations or multi-quark clusters. These effects can increase the high-momentum tail of the spectral function considerably compared to that expected for a simple Fermi-gas model. The Liuti aluminum cross section calculations were divided by a similar PWIA calculation for deuterium [23] to obtain the solid curves shown in Fig. 4. The curves generally reproduce all the trends in the data, but the predicted ratios at high x are larger than the experimental ones. This discrepancy may be reduced when FSI are included. The present data do not extend above $x = 1.3$, where Frankfurt and Strikman [24] predict that the ratio of cross sections for any two different nuclei should become constant if short-range correlations dominate. This prediction seems to be confirmed [24] in the range $1.3 < x < 1.8$ for the NE3 data [3] for D, He, C, Fe, and Au. The ratios of C/D and Fe/D are consistent with a constant value of about 5 in this x range. These data are mostly at $Q^2 < 2.5$ (GeV/c)^2, where the quasielastic channel dominates. It would be interesting to extend measurements of these cross section ratios to higher Q^2, where the resonance region inelastic channel will dominate.

IV. RESULTS FOR R

The present set of data includes measurements taken at both forward and backward angles, allowing the independent measurement of W_1 and W_2, or equivalently σ_T and R, in the large x and Q^2 region for a heavy nucleus. Using the second set of variables, R was extracted by performing Rosenbluth separations on groups of data points at similar values of x and Q^2, but different values of photon longitudinal polarization ϵ. The experimental cross sections can be written as:

$$\sigma = \frac{d\sigma}{d\Omega dE'} = \Gamma\sigma_T(x,Q^2)[1+\epsilon R(x,Q^2)], \tag{4.1}$$

where the virtual photon flux is given by

$$\Gamma = \frac{\alpha}{4\pi^2}\frac{(2M\nu - Q^2)E'}{Q^2ME}\frac{1}{1-\epsilon}, \tag{4.2}$$

and $R(x,Q^2)$ can be found from the slope of σ/Γ as a function of ϵ at common values of x and Q^2. Since the experimental spectra only have common values of Q^2 at the quasielastic peaks ($x = 1$), interpolations to common values of Q^2 away from the quasielastic peak were done using the same aluminum cross section model used for the radiative corrections. These corrections ranged from about 0.9 to 1.1. The extracted values of $R(x,Q^2)$ are shown as a function of x for five values of Q^2 in Fig. 5. Separations could not be made for $Q^2 = 6$ and 7 $(\mathrm{GeV/c})^2$ because spectra were only taken at one angle. The error bars are statistical only. Systematic errors are small in comparison, because overall normalization errors affect the forward- and backward-angle data equally, and the statistical errors on the backward-angle data are much larger than the point-to-point systematic errors. For each Q^2 value, no x-dependence is evident over the limited x range where separations were made. Also shown in Fig. 5 are two measurements [16] of R in deep-inelastic kinematics for hydrogen. The present high-x data have larger errors, but are consistent with the deep-inelastic results.

The average values of R at each Q^2 are shown as the solid lines in Fig. 5 and are plotted as a function of Q^2 in Fig. 6. It can be seen that R decreases with Q^2, becoming consistent with zero for $Q^2 > 3$ (GeV/c)^2. Also shown in Fig. 6 are the predictions of the simplified PWIA quasielastic model (Eq. 3.2) using form factor scaling (solid curve, same as Eq. 3.3), and the GK [20] form factor parametrization (dotted curve). The data are consistent with both curves, including the solid curve which was used in Section III to the extract values of νW_2 from the measured cross sections. The magnitude and Q^2 dependence of the new data for R for aluminum near $x = 1$ are quite similar to the values at lower x measured in deep-inelastic kinematics [16]. This may be further indication of the duality between the deep-inelastic and resonance regions. The relatively small values of R also indicate that scattering from spin-0 constituents, such as di-quarks, is not dominant. For example, the di-quark calculation of Abbott, Atwood, and Barnett [25] at $Q^2 = 5$ (GeV/c)^2 and $x = 0.8$ predicts $R = 0.35$. The di-quark calculation of Ekelin and Fredriksson [26] predicts an even larger value, $R = 0.45$, at the same kinematics. For comparison, the pQCD prediction (with target mass correction) [2] is $R = 0.12$. While these calculations do not necessarily apply to the present averages from $x = 0.8$ to $x = 1.2$, they do indicate that the inclusion of di-quarks could result in much larger values of R than seen in the present data. The present data are completely inconsistent with the simple quark-parton model Callan-Gross [27] relationship $F_2 = 2xF_1$. This simplifies at $x = 1$ to $R = 4M^2/Q^2$, and is almost a factor of ten larger than the present data. This relationship was also found [16] to give much larger values than both the data and the pQCD predictions in the deep inelastic region.

V. SUMMARY AND ACKNOWLEDGMENTS

The present data for electron scattering from aluminum are very well described by a recent microscopic model, and confirm the ξ scaling behavior seen in previous forward-angle. The scaling works considerably better in the region where inelastic resonance scattering dominates than in the region where quasielastic scattering dominates. The ratio of aluminum to deuterium cross sections exhibits considerable structure, most of which can be explained in a microscopic model. The inclusion of backward-angle data has permitted for the first time the measurement of R near $x = 1$ for $1.75 < Q^2 < 5$ (GeV/c)^2. The x-averaged values for R near the quasielastic peak decrease with increasing Q^2, and are consistent with expectations for quasielastic scattering in the PWIA.

We acknowledge the support of the SLAC management and staff, especially G. Davis, R. Eisele, C. Hudspeth, and J. Mark. We are grateful to S. Liuti for providing numerical calculations and for valuable discussions.

REFERENCES

a. Present address: Stanford Linear Accelerator Center, Stanford University, Stanford CA 94309.

1. E. Bloom and F. Gilman, Phys. Rev. **D4**, 2901 (1971).
2. A. De Rujula, H. Georgi, and H. D. Politzer, Ann. Phys. **103**, 315 (1977); H. Georgi and H. D. Politzer, Phys. Rev. **D14**, 1829 (1976); Phys. Rev. Lett. **36**, 1281 (1976).
3. D. B. Day *et al.,* Phys. Rev. Lett. **59**, 427 (1987).
4. S. Rock *et al.,* Phys. Rev. **D46**, 24 (1992).
5. B. W. Filippone *et al.,* Phys. Rev. **C45**, 1582 (1992).
6. C. Ciofi degli Atti, D. Day, and S. Liuti, submitted to Phys. Rev. **C** (1992).
7. Xiangdong Ji and B. W. Filippone, Phys. Rev. **C42**, R2279 (1990).
8. P. E. Bosted *et al.,* Phys. Rev. Lett. **68**, 3841 (1992).
9. A. Lung *et al.,* SLAC-PUB-5861, to be submitted to Phys. Rev. Lett.
10. P. N. Kirk *et al.,* Phys. Rev. **D8**, 63 (1973).
11. K. L. Brown, F. Rothacker, D. C. Carey, and Ch. Iselin, SLAC-Report-91, Rev. 2 (1977).
12. L. Andivahis *et al.,* SLAC–PUB–5753, to be submitted to Nucl. Instrum. Methods.
13. Y. S. Tsai, SLAC-PUB–848 Rev. (1971); see also L. W. Mo and Y. S. Tsai, Rev. Mod. Phys. **41**, 205 (1969).
14. A. A. Akhundov, D. Yu. Bardin, and N. M. Shumeiko, Sov. J. Nucl. Phys. **26(6)**, 660 (1977) and references therein.
15. S. Liuti, private communication. Calculations very similar to those presented in Ref. 6.

16. L. W. Whitlow *et al.,* Phys. Lett. **250**, 193 (1990); S. Dasu *et al.,* Phys. Rev. Lett. **61**, 1061 (1988).

17. I. McGee, Phys. Rev. **161**, 1640 (1967).

18. J. Gomez, Ph. D. Thesis, The American University, 1987; J. Gomez *et al.,* to be submitted to Phys. Rev. **C**.

19. A. Bodek *et al.,* Phys. Rev. **D20**, 1471 (1979).

20. M. Gari and W. Krümpelmann, Z. Phys. **A322**, 689 (1985).

21. C. Ciofi degli Atti, S. Liuti, and S. Simula, Phys. Rev. **C41**, R2474 (1990).

22. T. de Forest, Nucl. Phys. **A392**, 232 (1983).

23. S. Liuti, private communication. A more detailed study of cross section ratios at large x is in preparation.

24. L. Frankfurt and M. Strikman, in *Electromagnetic Interactions with Nuclei*, B. Frois and I. Sick, eds., World Scientific (1991).

25. L. F. Abbott, W. B. Atwood, and R. M. Barnett, Phys. Rev. **D22**, 582, 1980.

26. S. Ekelin and S. Fredriksson, Phys. Lett. **162B**, 373 (1985).

27. C. G. Callan and D. G. Gross, Phys. Rev. **D22**, 156 (1969).

FIGURE CAPTIONS

1. Values of $\nu W_2(\xi, Q^2)$ per nucleon for aluminum extracted from this experiment for the four forward-angle spectra taken at a beam energy of 5.5 GeV. The errors are statistical only, and do not include an overall normalization error of about 3%. The Q^2 values are at the quasielastic peak at $x = 1$, and vary slightly with ξ for each spectrum. The solid curves are from the calculations of Liuti [15], with the short dashed curves indicating the quasielastic contributions.

2. Same as Fig. 1 except for the four forward-angle spectra taken at $E = 9.8$ GeV.

3. Values of $\nu W_2(\xi, Q^2)$ per nucleon for aluminum as a function of Q^2 interpolated to $\xi = 0.6$, 0.7, 0.8, and 0.9. The data are for aluminum from this experiment (NE11), experiment E139 [18], and experiment E133 [4], and for iron from experiment NE3 [3]. The curves have the same meaning as in Figs. 1 and 2.

4. The ratios of cross sections per nucleon for aluminum compared to deuterium for the forward-angle data of this experiment (NE11) at $E = 5.5$ GeV and data at $\theta = 10°$ from experiment E133 [4]. The indicated Q^2 values are at $x = 1$. The solid curves are from the calculations of Liuti [23], with the short dashed curves indicating the quasielastic contributions.

5. Measured values (solid circles) of $R(x, Q^2)$ for aluminum as a function of x for five values of Q^2. The two crosses are for hydrogen [16] in the deep-inelastic region. The solid lines are the x-averaged values at each Q^2.

6. The x-averaged values of $R = \sigma_L/\sigma_T$ for aluminum from this experiment as a function of Q^2. The solid line is the PWIA quasielastic prediction (Eq. 3.2) using form factor scaling and $G_{En} = 0$. The dotted line is the prediction using the GK [20] form factor parametrization.

Table I. Cross section per nucleon for inelastic electron scattering from aluminum from this experiment. Also shown are values of $\nu W_2/A$ extracted assuming $R = 0.32/Q^2$. The errors are statistical only, and do not include an overall normalization error of about 3%.

E' (GeV)	Q^2 (GeV/c)^2	ϵ	x	ξ	$d\sigma/d\Omega dE'$ (nb/sr-GeV)	$\nu W_2/A$ ($\times$1000)
			$E = 1.968$	$\theta = 55.208$		
1.100	1.859	0.565	1.141	0.798	0.683 ± 0.042	15.7 ± 1.0
1.072	1.812	0.559	1.078	0.768	0.938 ± 0.037	22.1 ± 0.9
1.044	1.764	0.552	1.017	0.740	1.12 ± 0.04	26.9 ± 1.1
1.016	1.717	0.545	0.961	0.712	1.32 ± 0.09	32.3 ± 2.2
0.988	1.670	0.537	0.908	0.684	1.52 ± 0.13	37.9 ± 3.1
0.960	1.622	0.529	0.857	0.657	1.85 ± 0.11	46.8 ± 2.8
0.932	1.575	0.521	0.810	0.630	1.89 ± 0.17	48.7 ± 4.4
			$E = 2.407$	$\theta = 41.110$		
1.582	1.878	0.723	1.213	0.826	0.786 ± 0.111	9.47 ± 1.34
1.550	1.839	0.718	1.143	0.796	1.12 ± 0.12	13.9 ± 1.5
1.517	1.800	0.712	1.078	0.768	1.67 ± 0.07	21.5 ± 0.9
1.484	1.762	0.706	1.018	0.739	2.12 ± 0.07	28.0 ± 0.9
1.452	1.723	0.699	0.961	0.712	2.53 ± 0.07	34.3 ± 1.0
1.419	1.684	0.692	0.908	0.685	2.69 ± 0.13	37.5 ± 1.8
1.386	1.646	0.685	0.859	0.659	3.23 ± 0.12	46.2 ± 1.7
1.354	1.607	0.678	0.813	0.634	3.51 ± 0.11	51.4 ± 1.6
1.321	1.568	0.670	0.770	0.609	3.71 ± 0.13	55.4 ± 2.0
1.288	1.529	0.662	0.729	0.585	4.98 ± 0.77	75.9 ± 11.7
			$E = 2.407$	$\theta = 58.882$		
1.103	2.567	0.486	1.049	0.812	0.196 ± 0.018	11.3 ± 1.0
1.075	2.500	0.479	1.000	0.784	0.251 ± 0.016	14.7 ± 0.9
1.046	2.434	0.471	0.953	0.756	0.301 ± 0.021	17.7 ± 1.2
1.018	2.367	0.464	0.908	0.729	0.400 ± 0.041	23.7 ± 2.4
0.989	2.301	0.456	0.865	0.702	0.472 ± 0.033	28.1 ± 2.0
0.961	2.235	0.448	0.823	0.675	0.644 ± 0.047	38.5 ± 2.8
			$E = 2.837$	$\theta = 44.993$		
1.607	2.669	0.650	1.156	0.868	0.175 ± 0.025	5.69 ± 0.80
1.573	2.613	0.644	1.101	0.840	0.317 ± 0.026	10.5 ± 0.9
1.539	2.557	0.637	1.049	0.811	0.367 ± 0.020	12.3 ± 0.7

continued

Table I. continued.

E' (GeV)	Q^2 (GeV/c)^2	ϵ	x	ξ	$d\sigma/d\Omega dE'$ (nb/sr-GeV)	$\nu W_2/A$ (×1000)
1.505	2.500	0.630	1.000	0.784	0.485 ± 0.026	16.6 ± 0.9
1.471	2.444	0.623	0.953	0.757	0.576 ± 0.034	20.0 ± 1.2
1.437	2.387	0.616	0.909	0.730	0.583 ± 0.061	20.5 ± 2.2
1.403	2.331	0.608	0.866	0.704	0.793 ± 0.048	28.3 ± 1.7
1.369	2.275	0.600	0.826	0.679	0.992 ± 0.052	35.8 ± 1.9
1.335	2.218	0.591	0.787	0.654	1.12 ± 0.09	40.9 ± 3.2
			$E = 2.837$	$\theta = 61.205$		
1.155	3.397	0.438	1.076	0.867	0.0633 ± 0.0201	6.90 ± 2.19
1.130	3.323	0.432	1.038	0.842	0.0658 ± 0.0085	7.19 ± 0.93
1.105	3.250	0.426	1.000	0.819	0.0943 ± 0.0100	10.3 ± 1.1
1.080	3.177	0.420	0.964	0.795	0.120 ± 0.013	13.2 ± 1.4
1.055	3.104	0.414	0.928	0.772	0.0990 ± 0.0225	10.9 ± 2.5
1.030	3.030	0.408	0.894	0.748	0.157 ± 0.019	17.2 ± 2.1
1.006	2.957	0.401	0.860	0.726	0.182 ± 0.020	20.0 ± 2.2
0.981	2.884	0.394	0.828	0.703	0.203 ± 0.033	22.2 ± 3.6
			$E = 3.400$	$\theta = 34.694$		
2.146	2.594	0.761	1.102	0.839	0.574 ± 0.083	10.9 ± 1.6
2.107	2.547	0.756	1.050	0.811	0.704 ± 0.044	13.7 ± 0.9
2.068	2.500	0.750	1.000	0.784	0.912 ± 0.046	18.2 ± 0.9
2.029	2.453	0.744	0.953	0.757	0.880 ± 0.047	17.9 ± 1.0
1.990	2.406	0.737	0.909	0.731	1.20 ± 0.10	25.0 ± 2.0
			$E = 3.400$	$\theta = 44.482$		
1.700	3.311	0.615	1.038	0.842	0.137 ± 0.022	7.94 ± 1.24
1.668	3.250	0.609	1.000	0.819	0.139 ± 0.020	8.13 ± 1.16
1.637	3.189	0.602	0.964	0.795	0.194 ± 0.024	11.5 ± 1.4
1.605	3.128	0.596	0.929	0.773	0.233 ± 0.043	13.8 ± 2.6
			$E = 3.400$	$\theta = 57.572$		
1.289	4.066	0.441	1.027	0.862	0.0392 ± 0.0083	5.95 ± 1.26
1.260	3.972	0.435	0.989	0.836	0.0396 ± 0.0078	6.01 ± 1.19
1.230	3.878	0.428	0.952	0.810	0.0724 ± 0.0132	11.0 ± 2.0
			$E = 3.956$	$\theta = 28.409$		
2.709	2.581	0.830	1.103	0.838	0.686 ± 0.117	8.43 ± 1.43
2.666	2.541	0.825	1.050	0.811	1.01 ± 0.10	12.8 ± 1.2
2.624	2.500	0.820	1.000	0.784	1.25 ± 0.10	16.3 ± 1.3
2.581	2.460	0.815	0.954	0.758	1.35 ± 0.11	18.0 ± 1.5
2.539	2.419	0.810	0.910	0.732	1.41 ± 0.15	19.3 ± 2.0

continued

Table I. continued.

E' (GeV)	Q^2 (GeV/c)^2	ϵ	x	ξ	$d\sigma/d\Omega dE'$ (nb/sr-GeV)	$\nu W_2/A$ (×1000)
			$E = 3.956$	$\theta = 35.382$		
2.296	3.355	0.730	1.077	0.865	0.206 ± 0.048	7.26 ± 1.71
2.260	3.303	0.724	1.038	0.842	0.190 ± 0.030	6.78 ± 1.08
2.224	3.250	0.719	1.000	0.819	0.277 ± 0.035	10.0 ± 1.3
2.188	3.198	0.713	0.964	0.796	0.343 ± 0.040	12.6 ± 1.5
2.152	3.145	0.707	0.929	0.774	0.429 ± 0.058	16.0 ± 2.1
			$E = 3.956$	$\theta = 43.707$		
1.887	4.138	0.604	1.066	0.887	0.0655 ± 0.0252	5.67 ± 2.18
1.850	4.057	0.598	1.027	0.861	0.0655 ± 0.0126	5.72 ± 1.10
1.813	3.976	0.591	0.989	0.836	0.0555 ± 0.0111	4.87 ± 0.97
1.777	3.895	0.583	0.952	0.811	0.0887 ± 0.0161	7.84 ± 1.42
			$E = 3.956$	$\theta = 59.291$		
1.310	5.071	0.393	1.021	0.883	0.0086 ± 0.0033	2.23 ± 0.85
1.284	4.970	0.388	0.991	0.861	0.0187 ± 0.0047	4.81 ± 1.20
1.258	4.869	0.382	0.962	0.839	0.0236 ± 0.0060	6.05 ± 1.54
			$E = 4.507$	$\theta = 35.592$		
2.447	4.121	0.705	1.066	0.887	0.0969 ± 0.0354	5.42 ± 1.98
2.405	4.050	0.699	1.027	0.861	0.0977 ± 0.0190	5.54 ± 1.07
2.363	3.979	0.692	0.989	0.836	0.137 ± 0.022	7.84 ± 1.24
2.321	3.908	0.686	0.953	0.811	0.127 ± 0.023	7.34 ± 1.31
2.279	3.837	0.679	0.918	0.787	0.240 ± 0.058	14.1 ± 3.4
			$E = 4.507$	$\theta = 45.658$		
1.865	5.062	0.543	1.021	0.883	0.0173 ± 0.0062	2.67 ± 0.95
1.833	4.974	0.536	0.991	0.861	0.0150 ± 0.0055	2.32 ± 0.86
1.800	4.885	0.530	0.962	0.840	0.0395 ± 0.0097	6.10 ± 1.50
			$E = 5.507$	$\theta = 15.145$		
4.765	1.823	0.956	1.309	0.851	8.59 ± 1.21	11.0 ± 1.6
4.721	1.806	0.955	1.224	0.821	7.42 ± 0.82	10.1 ± 1.1
4.676	1.789	0.953	1.148	0.793	12.6 ± 1.0	18.0 ± 1.4
4.632	1.772	0.952	1.079	0.765	14.2 ± 1.0	21.4 ± 1.5
4.588	1.755	0.950	1.018	0.739	17.9 ± 1.1	28.3 ± 1.8
4.544	1.738	0.949	0.961	0.714	22.3 ± 1.2	36.8 ± 2.0

continued

Table I. continued.

E' (GeV)	Q^2 (GeV/c)^2	ϵ	x	ξ	$d\sigma/d\Omega dE'$ (nb/sr-GeV)	$\nu W_2/A$ (×1000)
4.499	1.721	0.947	0.910	0.689	23.9 ± 1.1	41.4 ± 2.0
4.455	1.704	0.945	0.863	0.666	25.2 ± 1.3	45.4 ± 2.3
4.411	1.687	0.943	0.820	0.643	26.3 ± 1.6	49.3 ± 3.1
4.367	1.670	0.941	0.781	0.622	30.4 ± 1.8	59.2 ± 3.5
4.322	1.654	0.939	0.744	0.601	31.3 ± 1.9	63.2 ± 3.8
4.278	1.637	0.936	0.710	0.581	32.1 ± 2.0	67.1 ± 4.3
4.234	1.620	0.934	0.678	0.562	36.0 ± 2.8	77.8 ± 6.0
4.189	1.603	0.931	0.648	0.543	33.7 ± 8.4	75.3 ± 18.7
			$E = 5.507$	$\theta = 18.981$		
4.466	2.674	0.927	1.369	0.956	0.390 ± 0.108	1.69 ± 0.47
4.417	2.645	0.925	1.294	0.925	0.794 ± 0.116	3.59 ± 0.52
4.369	2.616	0.923	1.225	0.895	0.949 ± 0.119	4.47 ± 0.56
4.320	2.587	0.921	1.162	0.866	1.35 ± 0.11	6.62 ± 0.54
4.272	2.558	0.918	1.104	0.837	1.75 ± 0.10	8.91 ± 0.51
4.223	2.529	0.915	1.050	0.810	2.70 ± 0.12	14.2 ± 0.6
4.175	2.500	0.913	1.000	0.784	2.80 ± 0.13	15.3 ± 0.7
4.126	2.471	0.910	0.954	0.758	3.06 ± 0.13	17.3 ± 0.7
4.078	2.442	0.907	0.911	0.734	3.85 ± 0.14	22.4 ± 0.8
4.029	2.413	0.904	0.870	0.710	4.61 ± 0.17	27.7 ± 1.0
3.981	2.384	0.901	0.832	0.687	4.76 ± 0.24	29.4 ± 1.5
3.932	2.355	0.897	0.797	0.665	5.87 ± 0.28	37.4 ± 1.8
3.884	2.326	0.894	0.764	0.644	6.72 ± 0.36	43.9 ± 2.3
3.836	2.297	0.890	0.732	0.623	8.06 ± 0.78	54.1 ± 5.2
			$E = 5.507$	$\theta = 22.804$		
3.907	3.363	0.875	1.120	0.889	0.406 ± 0.064	5.35 ± 0.84
3.863	3.326	0.871	1.078	0.865	0.505 ± 0.045	6.81 ± 0.60
3.819	3.288	0.868	1.038	0.841	0.604 ± 0.043	8.34 ± 0.60
3.775	3.250	0.865	1.000	0.819	0.743 ± 0.046	10.5 ± 0.6
3.731	3.212	0.861	0.964	0.796	0.841 ± 0.043	12.1 ± 0.6
3.688	3.175	0.858	0.930	0.775	0.959 ± 0.045	14.1 ± 0.7
3.644	3.137	0.854	0.897	0.754	1.00 ± 0.05	15.1 ± 0.8
3.600	3.099	0.850	0.866	0.734	1.26 ± 0.07	19.2 ± 1.1
3.556	3.061	0.846	0.836	0.714	1.48 ± 0.09	23.0 ± 1.4
3.512	3.024	0.841	0.808	0.694	1.64 ± 0.11	26.0 ± 1.7
3.468	2.986	0.837	0.781	0.676	2.13 ± 0.25	34.4 ± 4.0

continued

Table I. continued.

E' (GeV)	Q^2 (GeV/c)^2	ϵ	x	ξ	$d\sigma/d\Omega dE'$ (nb/sr-GeV)	$\nu W_2/A$ ($\times$1000)
			$E = 5.507$	$\theta = 26.823$		
3.508	4.157	0.818	1.108	0.913	0.0717 ± 0.0250	2.13 ± 0.74
3.459	4.099	0.813	1.066	0.886	0.114 ± 0.015	3.45 ± 0.44
3.410	4.041	0.808	1.027	0.861	0.156 ± 0.015	4.81 ± 0.45
3.361	3.983	0.803	0.989	0.836	0.221 ± 0.015	6.93 ± 0.47
3.312	3.925	0.798	0.953	0.812	0.267 ± 0.013	8.51 ± 0.42
3.263	3.867	0.793	0.918	0.788	0.321 ± 0.015	10.4 ± 0.5
3.214	3.809	0.787	0.885	0.765	0.413 ± 0.020	13.6 ± 0.6
3.165	3.750	0.781	0.853	0.743	0.495 ± 0.024	16.5 ± 0.8
3.116	3.692	0.775	0.823	0.721	0.548 ± 0.038	18.5 ± 1.3
			$E = 5.507$	$\theta = 32.829$		
2.913	5.124	0.713	1.052	0.905	0.0378 ± 0.0079	2.89 ± 0.60
2.871	5.051	0.708	1.021	0.883	0.0586 ± 0.0085	4.52 ± 0.65
2.830	4.978	0.703	0.991	0.861	0.0588 ± 0.0083	4.57 ± 0.64
2.789	4.906	0.697	0.962	0.840	0.0830 ± 0.0103	6.50 ± 0.81
2.748	4.833	0.691	0.933	0.819	0.0875 ± 0.0137	6.90 ± 1.08
			$E = 9.800$	$\theta = 13.248$		
7.900	4.121	0.952	1.156	0.938	0.260 ± 0.076	1.57 ± 0.46
7.837	4.088	0.950	1.110	0.911	0.589 ± 0.091	3.66 ± 0.57
7.775	4.056	0.949	1.067	0.886	0.696 ± 0.091	4.47 ± 0.58
7.712	4.023	0.947	1.027	0.860	0.860 ± 0.098	5.68 ± 0.65
7.650	3.990	0.945	0.989	0.836	1.07 ± 0.11	7.24 ± 0.73
7.587	3.958	0.943	0.953	0.813	1.16 ± 0.11	8.10 ± 0.80
7.525	3.925	0.941	0.919	0.790	1.42 ± 0.13	10.1 ± 0.9
7.462	3.892	0.939	0.887	0.769	1.75 ± 0.16	12.8 ± 1.2
7.400	3.860	0.937	0.857	0.748	2.06 ± 0.21	15.5 ± 1.6
7.337	3.827	0.935	0.828	0.727	2.27 ± 0.42	17.5 ± 3.2

continued

Table I. continued.

E' (GeV)	Q^2 (GeV/c)^2	ϵ	x	ξ	$d\sigma/d\Omega dE'$ (nb/sr-GeV)	$\nu W_2/A$ (×1000)
			$E = 9.800$	$\theta = 15.367$		
7.351	5.151	0.927	1.121	0.949	0.131 ± 0.052	1.81 ± 0.71
7.293	5.110	0.925	1.086	0.926	0.176 ± 0.038	2.47 ± 0.54
7.235	5.069	0.923	1.053	0.904	0.150 ± 0.033	2.15 ± 0.47
7.176	5.029	0.921	1.021	0.882	0.199 ± 0.037	2.92 ± 0.54
7.118	4.988	0.918	0.991	0.861	0.289 ± 0.044	4.31 ± 0.65
7.060	4.947	0.916	0.962	0.841	0.383 ± 0.051	5.83 ± 0.78
7.002	4.906	0.914	0.934	0.821	0.682 ± 0.072	10.6 ± 1.1
6.944	4.866	0.911	0.908	0.802	0.644 ± 0.078	10.2 ± 1.2
6.885	4.825	0.909	0.882	0.783	0.802 ± 0.109	12.9 ± 1.7
6.827	4.784	0.906	0.858	0.765	0.784 ± 0.219	12.8 ± 3.6
			$E = 9.800$	$\theta = 17.515$		
6.802	6.181	0.896	1.099	0.956	0.0265 ± 0.0100	0.730 ± 0.275
6.748	6.132	0.893	1.071	0.936	0.0643 ± 0.0125	1.80 ± 0.35
6.694	6.083	0.891	1.044	0.917	0.0873 ± 0.0131	2.48 ± 0.37
6.640	6.034	0.888	1.018	0.898	0.122 ± 0.015	3.51 ± 0.43
6.587	5.985	0.885	0.993	0.880	0.107 ± 0.014	3.13 ± 0.41
6.533	5.936	0.883	0.968	0.862	0.127 ± 0.016	3.75 ± 0.46
6.479	5.888	0.880	0.945	0.844	0.157 ± 0.018	4.71 ± 0.54
6.425	5.839	0.877	0.922	0.827	0.189 ± 0.022	5.73 ± 0.66
6.371	5.790	0.874	0.900	0.810	0.234 ± 0.029	7.20 ± 0.91
6.317	5.741	0.871	0.878	0.794	0.285 ± 0.052	8.87 ± 1.62
			$E = 9.800$	$\theta = 19.753$		
6.203	7.154	0.855	1.060	0.944	0.0328 ± 0.0107	1.68 ± 0.55
6.154	7.097	0.852	1.037	0.927	0.0250 ± 0.0085	1.29 ± 0.44
6.104	7.040	0.849	1.015	0.910	0.0433 ± 0.0108	2.26 ± 0.57
6.055	6.983	0.846	0.994	0.894	0.0415 ± 0.0106	2.19 ± 0.56
6.005	6.926	0.843	0.973	0.877	0.0679 ± 0.0137	3.62 ± 0.73
5.956	6.869	0.840	0.952	0.862	0.0689 ± 0.0145	3.70 ± 0.78
5.906	6.812	0.836	0.932	0.846	0.0728 ± 0.0166	3.95 ± 0.90
5.857	6.755	0.833	0.913	0.831	0.100 ± 0.023	5.49 ± 1.28
5.807	6.698	0.830	0.894	0.816	0.142 ± 0.044	7.82 ± 2.44

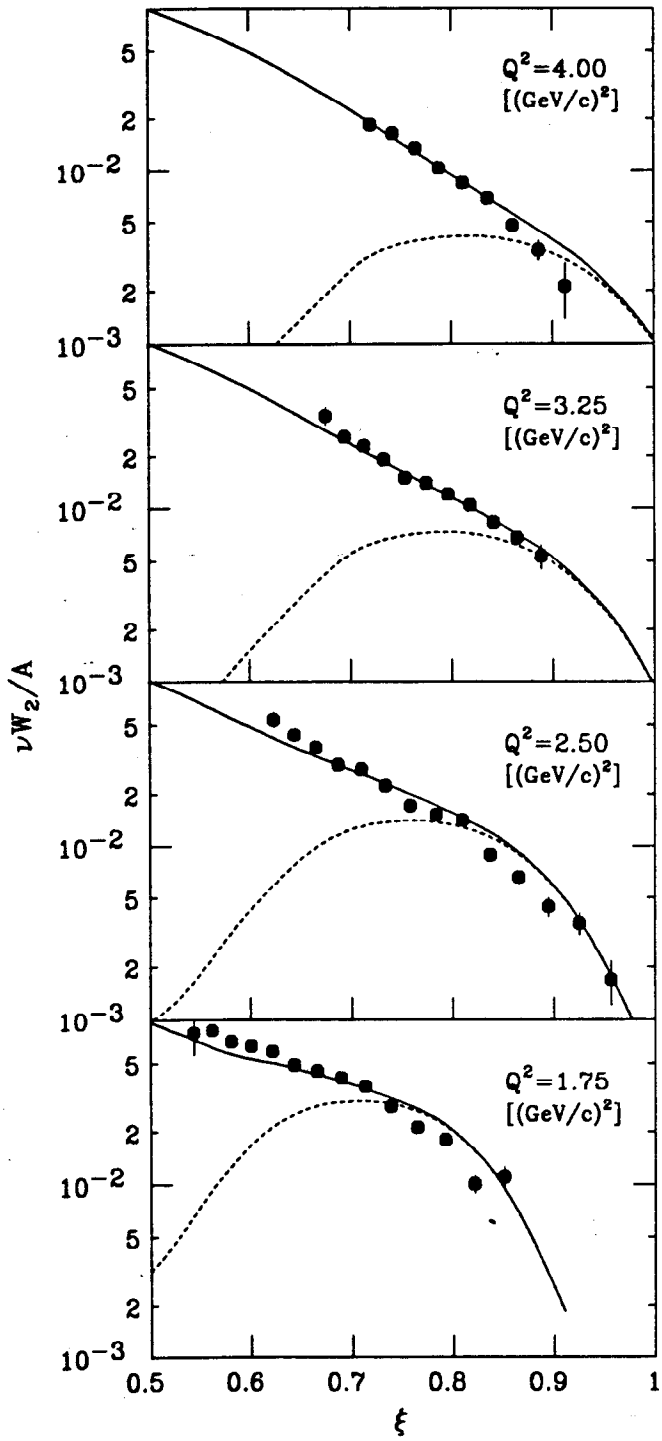
Q^2=4.00
[(GeV/c)^2]
Q^2=3.25
[(GeV/c)^2]
Q^2=2.50
[(GeV/c)^2]
Q^2=1.75
[(GeV/c)^2]
$\nu W_2/A$
ξ
10^{-2}
10^{-3}
0.5
0.6
0.7
0.8
0.9
1

Fig. 1

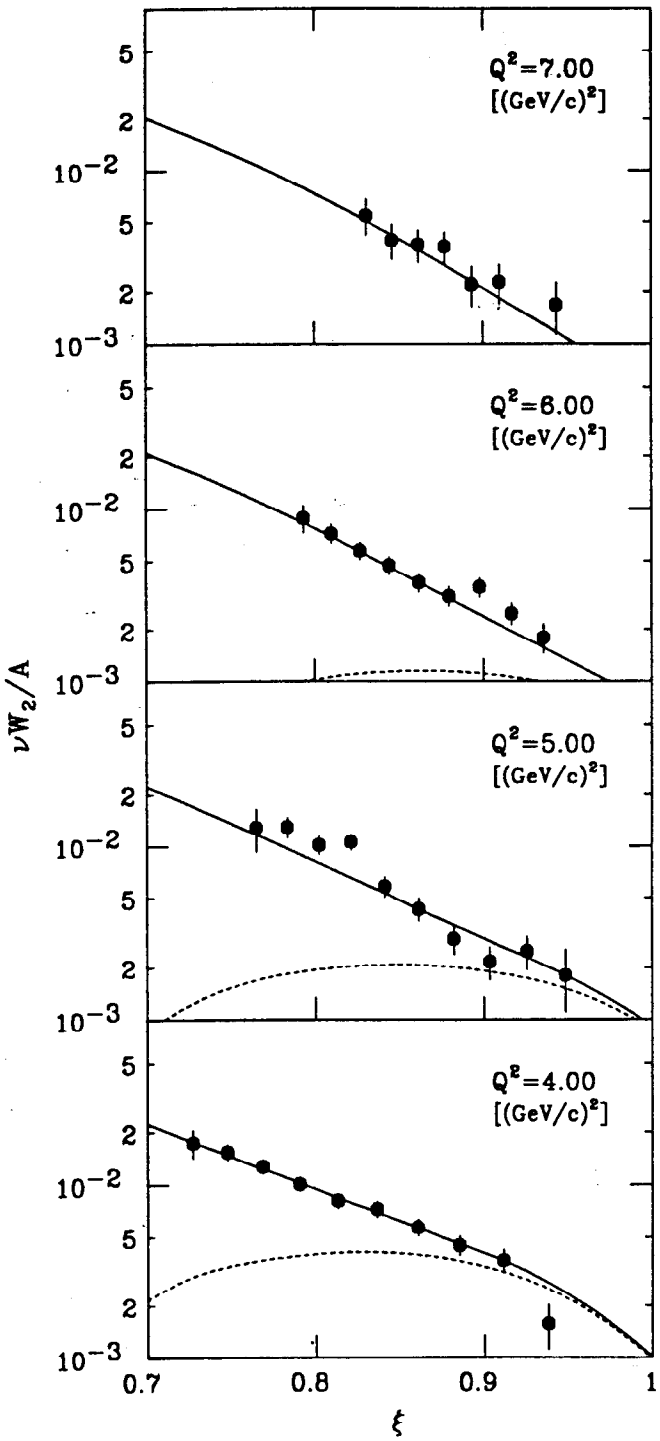
Q^2=7.00
[(GeV/c)^2]
Q^2=6.00
[(GeV/c)^2]
Q^2=5.00
[(GeV/c)^2]
Q^2=4.00
[(GeV/c)^2]
$\nu W_2/A$
ξ
10^{-2}
10^{-3}
0.7
0.8
0.9
1

Fig. 2

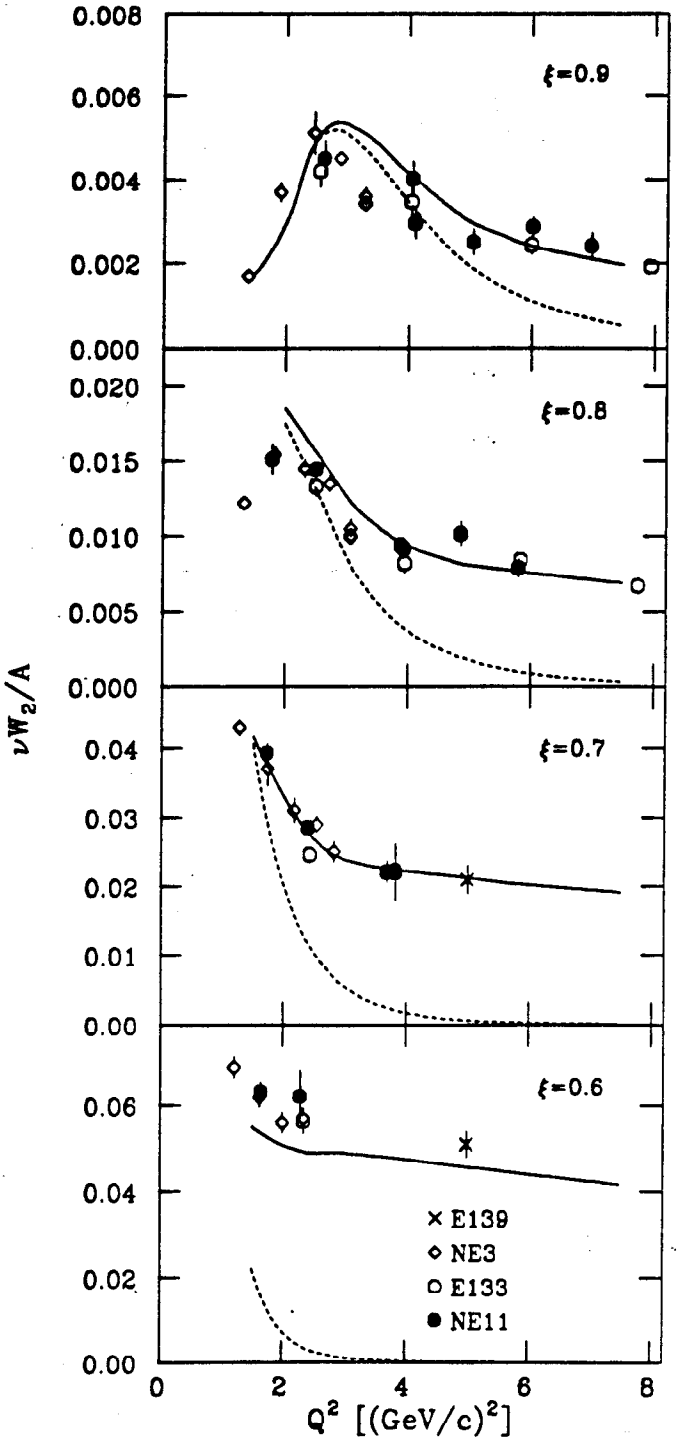
0.008
0.006
0.004
0.002
0.000
ξ=0.9
0.020
0.015
0.010
0.005
0.000
ξ=0.8
0.04
0.03
0.02
0.01
0.00
ξ=0.7
0.06
0.04
0.02
0.00
ξ=0.6
× E139
◇ NE3
○ E133
● NE11
νW2/A
0
2
4
6
8
Q² [(GeV/c)²]

Fig. 3

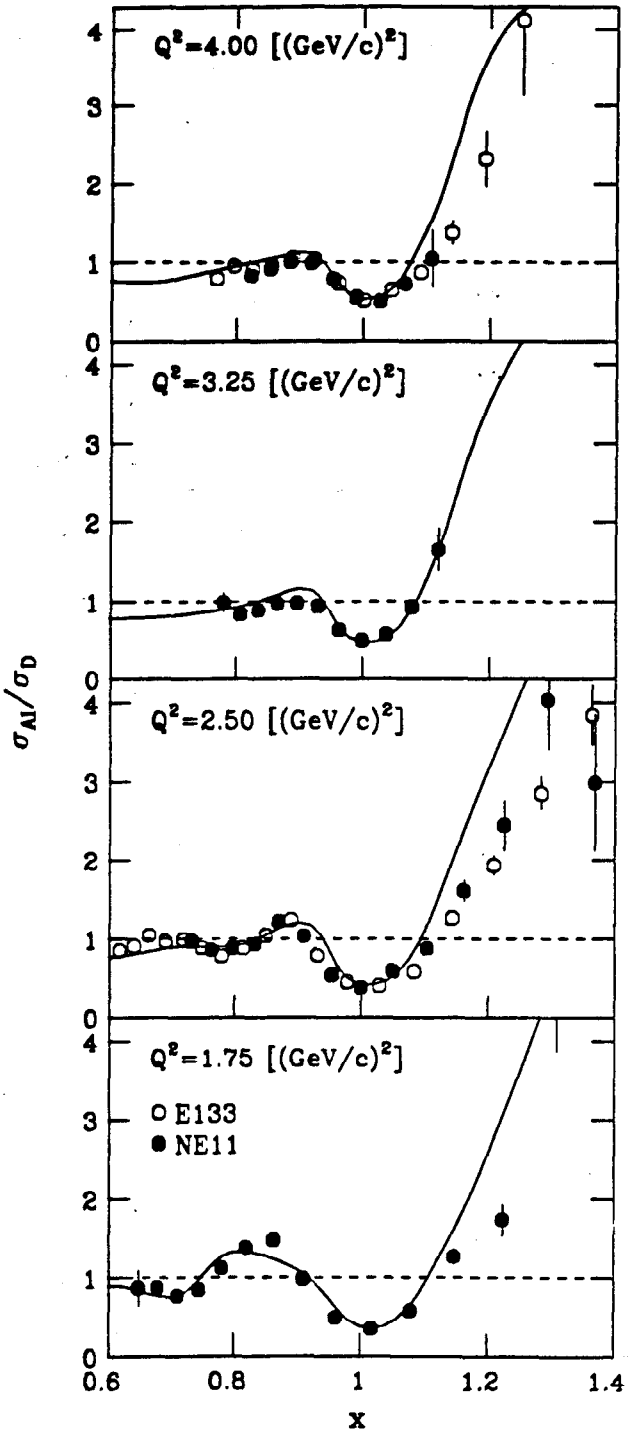
Q^2=4.00 [(GeV/c)^2]
Q^2=3.25 [(GeV/c)^2]
Q^2=2.50 [(GeV/c)^2]
Q^2=1.75 [(GeV/c)^2]
E133
NE11
σ_{Al}/σ_D
x
0
1
2
3
4
0.6
0.8
1
1.2
1.4

Fig. 4

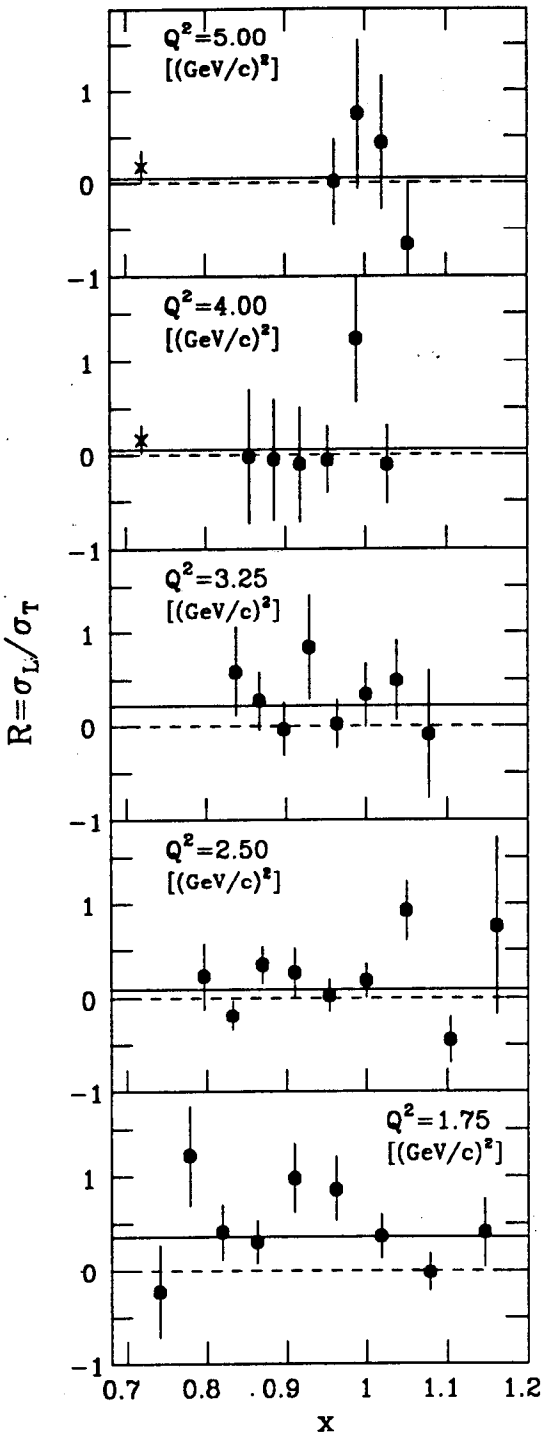
Q^2=5.00
[(GeV/c)^2]
Q^2=4.00
[(GeV/c)^2]
Q^2=3.25
[(GeV/c)^2]
Q^2=2.50
[(GeV/c)^2]
Q^2=1.75
[(GeV/c)^2]
$R=\sigma_L/\sigma_T$
x
0.7
0.8
0.9
1
1.1
1.2

Fig. 5

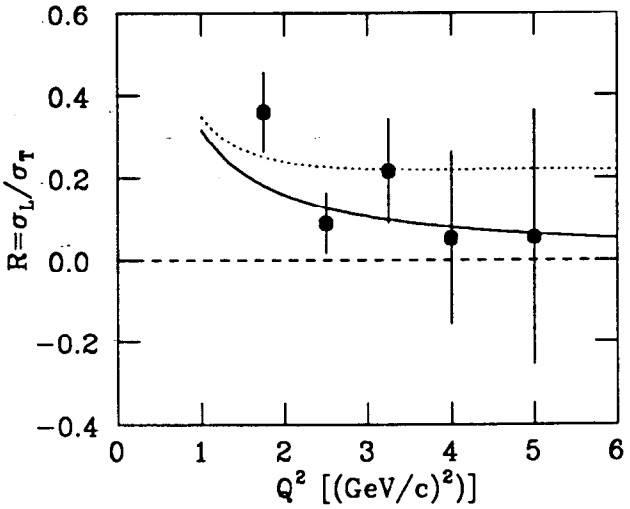

Fig. 6